RESEARCH PAPER

Peak broadening caused by using different micro–liquid chromatography detectors

Tobias Werres[1,2] · Torsten C. Schmidt[2] · Thorsten Teutenberg[1]

Abstract

Advancements in column technology resulted in smaller particles and more efficient phases. In parallel, the use of columns with reduced dimensions is becoming more common. This means the effective column volume is also decreased, thereby making the systems more susceptible to effects of band broadening due to extra-column volume. Despite these trends and the fact that a growing number of miniaturized liquid chromatography systems are being offered commercially, manufacturers often stick to the modular concept with dedicated units for pumps, column oven, and detectors. This modular design results in long connection capillaries, which leads to extra-column band broadening and consequently prevents the exploitation of the intrinsic efficiency of state-of-the-art columns. In particular, band broadening post column has a considerable negative effect on efficiency. In this study, mass flow and concentration-dependent detectors were examined for their influence on band broadening using a micro-LC system. A mass spectrometric detector, an evaporative light scattering detector, two UV detectors, and a previously undescribed fluorescence detector were compared. The influence on efficiency is compared using plate height vs linear velocity data and peak variance. It is shown that an increase in the inner diameter after the post-column transfer capillary leads to significant loss in plate height. Comparing the UV detectors, it could be shown that the dispersion was reduced by 38% by the reduction of the post-column volume. The largest variance was found for the evaporative light scattering detector, which was 368% higher compared to the variance of the detector with the least effect on band broadening.

Keywords Miniaturization · Extra-post-column band broadening · Micro bore column · Apparent efficiency

Abbreviations

ECBB	Extra-column band broadening
CFD	Computational fluid dynamics
ELSD	Evaporative light scattering detector
FS	Fused silica

Introduction

Miniaturized LC systems are increasingly gaining both relevance and acceptance in industry [1, 2]. In addition to the increasing availability of commercial systems, this is mainly due to the increased environmental awareness of the users and factors of profitability [3, 4]. Above all, the benefits of high ionization efficiencies, reduced matrix influence, and the capability to analyze the smallest sample volumes make miniaturized LC coupled to mass spectrometry the main driving force behind the spread of the technology [1, 2, 5–7]. The modular design of classical HPLC systems is based on the "HiFi Tower" principle and offers above all the advantage of high flexibility. However, in the context of microflow systems, adherence to this concept has one major drawback. Due to the modular design, longer flow paths are required that inevitably lead to a high extra-column volume. As a consequence, the intrinsic efficiency of modern sub-2-μm separation phases cannot be fully utilized [8, 9]. However, in current research, it can be observed that the trend is moving further toward miniaturized compact systems. Such a compact design results in a reduction of the extra-column band broadening (ECBB). A growing number of these "suitcase systems" with focus on reduction of ECBB have been presented by several research groups [10–12].

✉ Thorsten Teutenberg
teutenberg@iuta.de

1. Institut für Energie- und Umwelttechnik e. V., IUTA (Institute of Energy and Environmental Technology), Bliersheimer Str. 58-60, 47229 Duisburg, Germany

2. Instrumental Analytical Chemistry, University Duisburg-Essen, Universitätsstr. 5, 45141 Essen, Germany

Also, first approaches for ultra-low-cost miniaturized HPLC "for everybody" have already been proposed [13]. The rapid development of 3D printing will further accelerate this trend [14, 15].

While ECBB already has a significant effect on the resolving power of a separation in modern UHPLC systems using 2.1-mm-ID columns, the effect is even more pronounced when using micro bore columns with an ID of 300 μm as employed in micro-LC systems [16, 17]. The mismatch will become particularly relevant in the light of ongoing improvements in the field of chromatographic separation phases, where new standards of efficiency are being set with increasingly smaller particle diameters and narrower particle size distributions [18]. Overall, the ECBB can be divided into three parts: the injection volume and injection method, tubing and connectors, and the detector.

In our previous work, the influence of the injection volume and the injection technique on the chromatographic efficiency and the extra-pre-column band broadening was investigated. It was found that a fixed loop in combination with metered injection generates the highest efficiency [19]. Thanks to Taylor and Aris the influence of tubing on the flow profile of the mobile phase is well understood and described at least for unbent, circular-profiled connection tubing under laminar flow conditions [20, 21]. However, tubing in real systems is often bent or shows other "irregularities." This can, for example, result in so-called racetrack effects [22]. Thus, the determination of all possible factors that might cause significant band broadening in connecting tubing would have to be determined with, e.g., computational fluid dynamics (CFD) simulations [23]. Connections between individual HPLC components are potential sources for introducing ECBB but can nowadays be made with ultra-low dead volume connectors. Due to the diversity of detector designs and the associated changes in the inner diameters and turns of the flow path, no universal mathematical equation can be used for the prediction of the influence on the ECBB. The influence of the detector on the ECBB can only be determined by elaborate simulations or by experiments for each detector independently. Although miniaturized LC in combination with mass spectrometry is the preferred method for a variety of applications, there are no extensive studies on band dispersion using such a coupling.

Therefore, the aim of this investigation was to evaluate the influence of different detectors on the extra-post-column band broadening using sub-2-μm particles in columns with an ID of 300 μm. For this purpose, three concentration-dependent detectors and two mass flow–dependent detectors were investigated. Chromatographic performance was assessed by change in band spreading caused by the post-column connection tubing as well as the specific detector.

Other variables were kept constant. These comprise the injector, the injection method, the injection volume, the pre-column tubing, and the column itself. Among the concentration-dependent detectors, two diode-array detectors (DAD) and a fluorescence detector (FLD) were included. The mass flow–dependent detector was represented by an evaporative light scattering detector (ELSD) and an ESI–MS, where the influence of the emitter capillary ID on band broadening is discussed in detail.

Materials and methods

Chemicals and reagents

Water and acetonitrile of LC–MS grade as well as acetone for the determination of the system dwell times were purchased from Th. Geyer (Chemsolute, Renningen, Germany). Formic acid (Sigma-Aldrich, Seelze, Germany) was added to a total volume concentration of 0.1% to the mobile-phase solvents. Uracil was used to determine the column void time and purchased from Sigma-Aldrich. Naproxen (Sigma-Aldrich) was chosen as the model analyte because it generated a sufficient signal for all investigated detectors.

HPLC setup

All experiments were done on an Eksigent ExpressLC Ultra system (Sciex, Dublin, CA, USA). The system can be operated up to a maximum pressure of 690 bar. For sample loading, an HTS PAL autosampler (CTC Analytics, Zwingen, Switzerland) was used. Sample injection onto the column was carried out by the integrated six-port-two-position valve and via fixed sample loop (PEEKsil™ 75 μm × 10 cm) by means of metered injection. A YMC-Triart C18 column with a length of 50 mm and an ID of 0.3 mm packed with fully porous 1.9-μm particles with a pore size of 120 Å and 1/32″ connectors was used and operated at 50 °C (YMC Europe GmbH, Dinslaken, Germany).

For connecting tubing, fused silica (FS) capillaries (Postnova Analytics, Germany) with an outer diameter of 360 μm and an inner diameter of 50 μm were used. The FS capillaries were cut to the required length using the Shortix™ Tubing Cutter (Supelco, Bellefonte, PA, USA). Furthermore, the cutting edges of the capillaries were further processed using the Capillary Polishing Station (ESI Source Solution, Woburn, MA, USA) using diamond lapping film with a 1-μm grade to obtain a mirror-smooth surface. Finally, the capillaries were rinsed to remove grinding residues. EXP®2 TI-LOK™ Hand-Tight Adapters (Optimize Technologies, Oregon City, OR, USA) were used to guarantee a dead volume free connection of the system components.

Detectors

Several detectors were used for comparison of the influence on the band broadening. Both DAD studied in this work had a U-shaped cell, but still differed in their conceptual implementation in some details. The first UV detector (DAD 1) was the AZURA DAD 2.1L (Knauer, Berlin, Germany) equipped with a nano UV flow cell with a volume of 6 nL and an effective light path of 3 mm. The cell consisted of a single continuous FS capillary with an inner diameter of 50 μm. The cell can be decoupled and placed directly behind the column using light wave guides. Therefore, this detector had the smallest post-column volume of about 200 nL. The absorbance was recorded with a sampling rate of 20 Hz and a wavelength of 275 nm was chosen. A spectral band width of 4 nm was selected.

The second UV detector (DAD 2) with a cell volume of 80 nL and an effective light path of 6 mm was a 1260 Infinity II DAD WR (Agilent Technologies, CA, USA). The detector follows the classical "HiFi Tower" approach. The connection is made via a 400-mm × 0.05-mm pre-cut PEEKsil™ capillary, which can be connected to the cell without dead volume due to a special conical cut. The ID of the cell increased to 130 μm, resulting in a total detector post-column volume of 865 nL. The absorbance was recorded with a data sampling rate of 20 Hz and a wavelength of 275 nm was chosen. A spectral band width of 4 nm was selected.

As FLD, the NanoFLD (Dr. Licht GmbH, Nümbrecht, Germany, Art. LO116) was used. Recording of the signal was performed via the integrated single-board computer (Raspberry Pi 4) which resulted in sampling rates up to 10 Hz. For excitation of the sample, a UV-C LED with a wavelength of 275 nm was used. The emitted light was recorded using a photomultiplier equipped with a wide band filter that cuts all wavelengths < 305 nm. The flow cell consisted of a 6-cm-long stripped FS capillary with an ID of 50 μm which resulted in the largest cell volume of 117 nL of the concentration-dependent detectors investigated. Two centimeters of the cell, corresponding to 39 nL, was located in the so-called Ulbricht sphere for efficient light collection. The total volume of the assembly is 530 nL without

the swept volume of the T-pieces. Connection to the optical fibers and the column outlet is achieved using T-pieces (IDEX; U-428; swept volume of 0.57 μL). A description of this detector can be found in Supplementary S 2.

For the MS measurements, a QTrap 3200 mass spectrometer (Sciex, Dublin, CA, USA) was used. To characterize the band broadening, three different emitter capillaries with an inner diameter of 65 (MS 65), 50 (MS 50), and 25 μm (MS 25) were used. While the 65-μm-ID emitter capillary was made of stainless steel, the emitter capillaries with a smaller ID are based on a PEEKsil™ capillary with stainless steel tip. The signal intensity of naproxen was recorded by multiple reaction monitoring at m/z 229.0 –> 113.0 and a dwell time of 40 ms. The following source parameters were used: declustering potential, − 20 V; entrance potential, − 10 V; collision energy, − 30 V; collision cell exit potential, − 5 V; curtain gas, 10 psi; ion spray voltage, 4.2 kV; ion source gas 1, 20 psi; and temperature, off.

As an evaporative light scattering detector (ELSD), the ELSD 85LT (Knauer, Berlin, Germany) equipped with a special nebulizer and glassware chamber for the flow rate range of 5 to 40 μL/min was used. A sampling rate of 30 Hz with a gain of 12 and a filter time of 1 s was selected.

Since there is no classical cell volume in the mass flow–dependent detectors which influences the band broadening, it must be clearly differentiated which transport mechanism is used for the analytes after the transition into the gas phase. For ESI–MS, ions are generated from the analyte molecules which are subsequently transported through an electric field. An optimized ion source design has thus only influence on the sensitivity. When using an ELSD, a desolvation step is carried out after nebulization. Afterwards, the desolvated analyte particles are transported by a gas stream. During this process, further band broadening can take place.

Table 1 summarizes the most important dimensions and volumes of the individual detectors. The calculations were based on the nominal inner capillary diameters as specified by the manufacturers.

Figure 1 shows the schematic of the cell detector geometries. Care was taken to maintain the ratio of the capillary diameters to each other.

Table 1 Summary of the dimension and volume of additional connectors needed of the studied detectors and their acronym in the further document

Detector	Acronym	Tubing mm × mm (nL)	Cell/emitter/desolvation mm × mm (nL)	Union/T-pieces Amount (nL)	Total
AZURA DAD 2.1L	DAD 1	100 × 0.05 (196)	3 × 0.05 (6)	0/0	202
1260 Infinity II DAD WR	DAD 2	400 × 0.05 (785)	6 × 0.13 (80)	0/0	865
NanoFLD	FLD	210 × 0.05 (412)	60 × 0.05 (117)	0/2 (570)	1169
QTrap 3200	MS 25 μm	210 × 0.05 (412)	215 × 0.025 (105)	1/0	517
	MS 50 μm	210 × 0.05 (412)	215 × 0.05 (422)	1/0	834
	MS 65 μm	210 × 0.05 (412)	215 × 0.065 (713)	1/0	1125
ELSD 85LT	ELSD	250 × 0.05 (490)	– (2570)	1/0	3060

Fig. 1 Schematic representation of the investigated detector configurations. Ratios of the capillary IDs were retained. A detailed explanation of the cell design of the FLD can be found in Supplementary S1
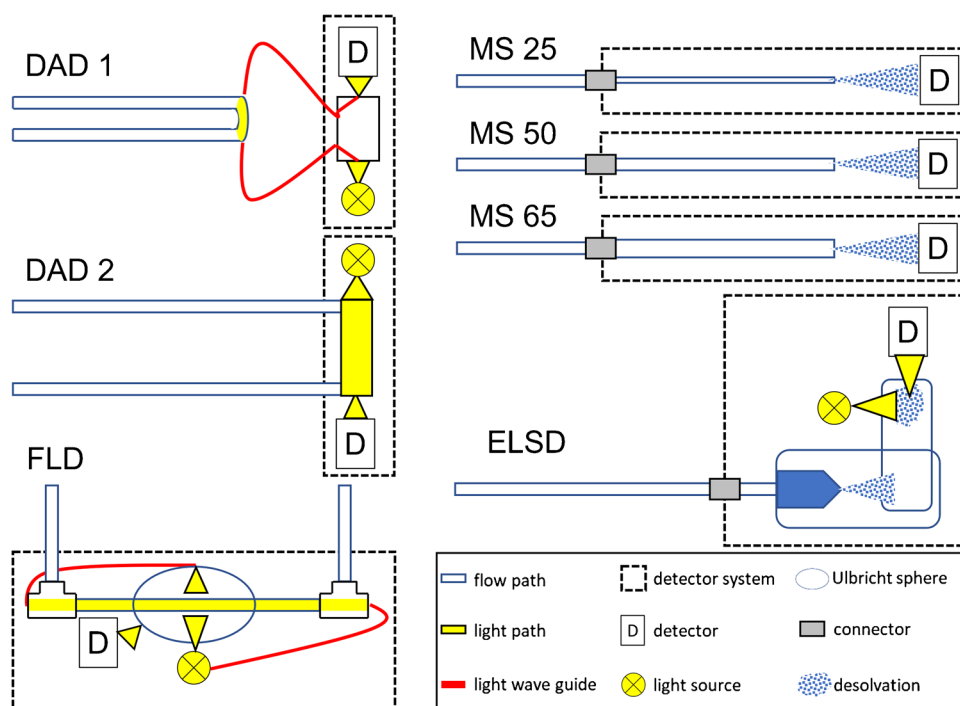
Determination of plate height and peak variance

For the determination of the plate height and peak variance (σ^2), the peak widths were measured at half height. This procedure is only valid if the peaks are symmetrical. Depending on the flow rate, a peak symmetry between 1.2 and 0.9 could be determined for all detectors investigated apart from the ELSD. To prevent peak dispersion due to volume overload, 100 nL of a 150-µg/mL naproxen sample was injected into the system. The mobile phase was set to 47% B to adjust the retention factor (k) of naproxen to 2. A retention factor of 2 was chosen because extra-column band broadening has a significant effect on weakly retained analytes. The flow rate was varied between 2 and 25 µL/min. All measurements were performed in triplicate.

Software and data processing

The micro-HPLC was controlled via Eksigent Control Software Version 4.2 Build 151,019–1321 (Sciex, Dublin, USA). Data acquisition for the Agilent detector was performed using Open LAB CDS Rev.C.0107.SR3 (Agilent Technologies, CA, USA). The detectors from Knauer were operated with Clarity Chrome® version 8.1.0.87 Build Mar 28 2019 (Knauer, Berlin, Germany). The FLD was controlled by means of a python script (Dr. Licht GmbH, Nümbrecht, Germany), and the MS data was acquired using Analyst® 1.6.3 Build 5095 (Sciex, Dublin, USA). Further data processing was performed using OriginPro 2019b (64-bit) 9.6.5.169 (OriginLab, MA, USA) and Microsoft Office Excel 2010.

The peak widths were determined using the Peak Analyzer from OriginPro.

Results and discussion

Comparison of the influence of the detectors on extra-post-column band broadening

The visualization of the influence of the investigated detectors on the extra-post-column band broadening was done by volume peak dispersion [19, 24]. Here, the time-dependent peak widths are transformed into volume-dependent dispersion. The transfomation was done using the following equation:

$$\sigma^2 = \left(\frac{w_h}{2.355} * F \right)^2 \tag{1}$$

where σ^2 is the peak variance; w_h, the full width at half maximum (FWHM) of the peak; and F, the flow rate.

Figure 2 shows the comparison of the different detectors on the efficiency of the system. Additionally, plate height (H) vs linear velocity (u_0) plots are shown to further discuss the observed effects [17, 25].

As Fig. 2a shows, a significant increase in peak variance at the highest investigated flow rate of 25 µL min^{-1} was observed when the ESI–MS emitter capillary with an ID of 65 µm, the ELSD, or the FLD was used. The system configurations have in common that after the transfer capillary
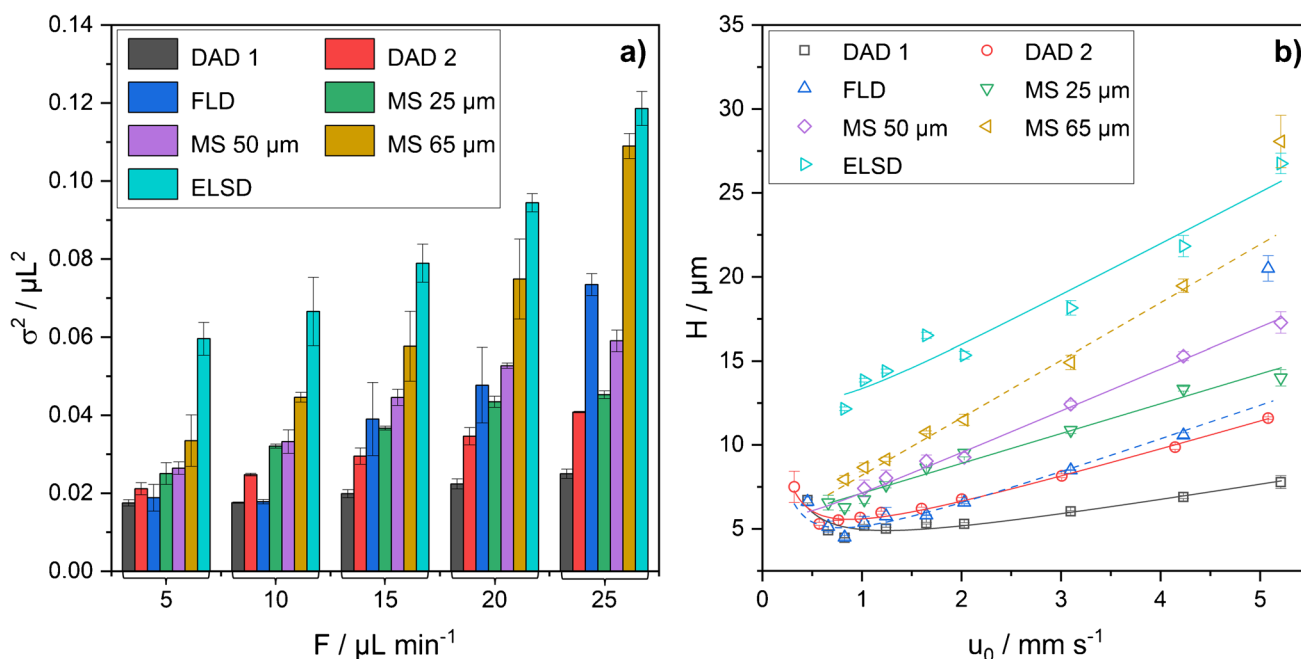
Fig. 2 Comparison of the influence of the studied detectors on the extra-post-column band broadening in two visualizations. **a** Dependence of the peak variance at different flow rates. **b** Comparison of the resulting H vs u_0 plots. Solid lines represent the fit calculated by the residual sum of squares method for the experimental values. The dotted lines represent the fit if the last data point is omitted. Error bars indicate the standard deviation calculated for $n = 3$

with an ID of 50 µm connecting the column outlet to the detector, there is a change to a larger ID of 65 µm for the ESI–MS emitter capillary and 500 µm for the T-piece of the FLD. When laminar flow occurs in a capillary, diffusion in the radial direction counteracts band spreading. When the ID of the capillary is increased, the linear flow velocity decreases. In addition, areas of stagnant mobile phase form at the transition to the larger ID. The molecules migrate into and out of the stagnant regions by diffusion. At high linear flow velocities, the analyte molecules near the center of the capillary move so fast in the longitudinal direction that the time for rediffusion is no longer sufficient and band broadening occurs. This has the consequence that an unfavorable flow path geometry can lead to significant losses in efficiency, especially at high linear flow velocities. These observations are consistent with the study of Filip et al. who, using CFD, were able to simulate similar effects on the peak broadening when changing to higher IDs at high linear flow velocities [23].

The lowest peak variance was found for DAD 1, with an overall increase from 0.018 to 0.025 µL^2 (43%) in the observed flow rate range. The highest dispersion was found for the ELSD at a flow rate of 25 µL min^{-1} with 0.117 µL^2. The influence of the cell volumes for DAD 2 and the ESI–MS emitter capillaries with an ID of 25 µm and 50 µm on the variance is comparable. The highest increase in peak broadening at a flow rate of 25 µL/min was found for

the detectors with an increase of the inner diameter of the flow path after the transfer capillary. For the FLD and the ESI–MS emitter capillary with an ID of 65 µm, the increase was 290% and 225%, respectively.

The peak variance can be correlated with the post-column volume when the detectors are separated into concentration-dependent detectors and mass flow–dependent detectors. In the case of the FLD, the large change in variance can be explained by the significant increase in the inner diameter from 50 to 500 µm (see Fig. 1). In conclusion, it can be stated that a constant diameter of the flow path after the column as well as the reduction of the ID after the transfer capillary had no negative influence on the band broadening. By changing to a larger ID, deviations from the expected data patterns could be identified at high flow rates. For DAD 2, where the change to the larger ID only occurred within the detector cell, this effect was not observed.

Comparing the H vs u_0 plots for the concentration-dependent detectors in Fig. 2b, there is no significant influence on H_{min}. The lowest $H_{min} = 4.9 \mu m$ was achieved with DAD 1. Considering all data points, an $H_{min} = 4.7 \mu m$ was calculated for the FLD, which is explained by the overestimation of the C-term by the fit function. Examining the dotted plot line of the FLD, an intersection with the plotline of DAD 2 is observed at 2.2 mm s^{-1}. Excluding the last data point results in an $H_{min} = 5.0 \mu m$. When using DAD 2, an $H_{min} = 5.5 \mu m$ was achieved. With increasing the ID

of the ESI–MS emitter capillary, the post-column volume increases and the linear flow velocity in the emitter capillary decreases. As a result, due to spray instabilities, it was not possible to represent H_{min} when using the ESI–MS emitter capillaries with an ID of 50 μm and 65 μm, and the ELSD. When using the ESI–MS emitter capillary with an ID of 25 μm, an $H_{min} = 6.2$ was observed.

The general assumption that the dispersion is a function of the post-column volume only reflects reality to a limited extent. The 25-μm-ID emitter capillary yields a comparable post-column volume as the detection cell of the FLD, and the emitter capillary with an ID of 50 μm has a comparable volume as the cell of the DAD 2, but the band broadening is clearly different. However, with increasing post-column volume, a correlation to an increase of the slope of the H vs u_0 plot at higher flow rates can be observed. As a result, only a small optimal flow rate range can be used despite the use of sub-2-μm particle packed stationary phases. The specific choice of the detector can thus prevent the use of methods with a high flow rate if the chromatographic resolution needs to be optimized.

Comparison of sensitivity and signal-to-noise ratio

To allow a direct comparison between the different detectors, the concentration of the model analyte was chosen to generate a signal with a signal-to-noise ratio > 5. The resulting normalized chromatograms of the concentration-dependent detectors are compared in Fig. 3.

Only under the assumption that turbulent mixing takes place in the detector cell can it be concluded that the square of the cell volume is equal to the peak variance
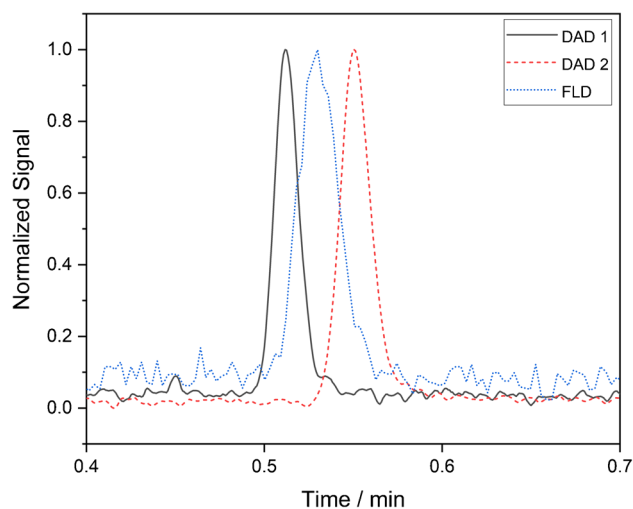

Fig. 3 Normalized chromatogram of naproxen at $k = 2$ for the concentration-dependent detectors. Column: YMC-Triart C18, 50×0.3 mm, 1.9 μm; temperature, 50 °C; injection volume, 100 nL; $F = 25$ μL min.$^{-1}$

[16]. In contrast, the inlets and outlets as well as the already discussed dead zones have a significant influence on the peak broadening. Based on the cell length of DAD 1 being only half as long compared to that of DAD 2, the signal intensity should be half as large. However, the resulting signal of DAD 1 is 8 times smaller, but at the same time, the signal-to-noise ratio is only 1.5 times lower (16 versus 24). On the other hand, the total dispersion of the system is reduced by 38% at a flow rate of 25 μL min^{-1}.

According to Lambert–Beer's law, the sensitivity of the UV detectors depends largely on the path length of the light beam through the sample. Nevertheless, other factors such as the light throughput play a decisive role. By increasing the ID of the cell, light coupling can be facilitated, but this increases the cell volume. Thus, while increasing the cell diameter has a positive effect on the detection limit, increasing the extra-post-column volume has a negative effect on band broadening and thus on the efficiency of the entire separation system. It is crucial to find the best balance between dispersion and sensitivity.

For the FLD, an S/N of only 6 was calculated under the same conditions. Comparing the total volumes of the concentration-dependent detectors in Table 1, the retention time of naproxen using the FLD should be higher than for DAD 2. This only allows the conclusion that not the entire swept volume of the T-piece contributes to the total volume of the detector. The chromatogram of the FLD clearly shows the issue of the low data sampling rate at higher flow rates. The undersampling that occurs because of the lower data acquisition rate of the FLD can lead to electronic peak broadening. To eliminate the described weaknesses regarding sensitivity while maintaining portability, an active cooling of the LED by means of a heat sink and fan should be implemented. These modifications should substantially increase the utilizable intensity of the LED, thus increasing the detection limit and significantly reducing the noise. In addition, the installed T-pieces must be replaced by more suitable ones with a smaller bore to reduce the swept volume. The normalized peaks for the mass flow–dependent detectors are shown in Fig. 4.

In the chromatogram of the ELSD, in addition to the peak broadening, a considerable tailing of the peak is evident. Using ESI–MS detection, it can be assumed that after the spraying of the mobile phase, the analyte peak does not experience any further dispersion [26]. In contrast to MS, in which ions are generated in the ion source and then transported through an electric field, in ELSD after nebulization in the microflow chamber, molecules are transported through a gas stream in a heated spiral to get fully desolvated and subsequently
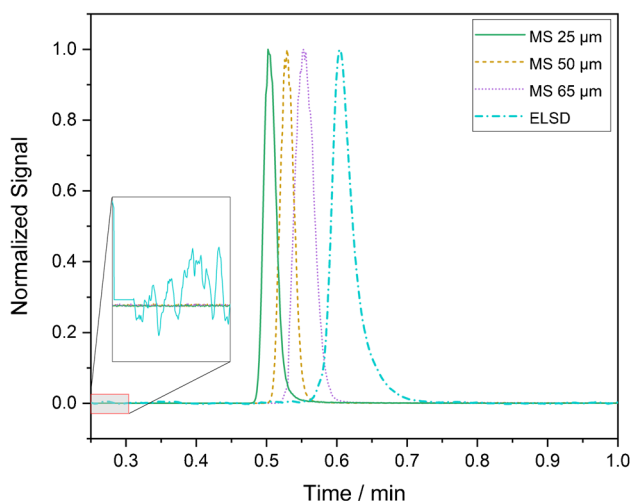
Fig. 4 Normalized chromatogram of naproxen at $k = 2$ with zoom in on the baseline for the mass flow–dependent detectors. Column: YMC-Triart C18, 50×0.3 mm, 1.9 μm; temperature, 50 °C; injection volume, 100 nL; $F = 25$ μL min.$^{-1}$

detected. Because of the nature of the technology, it is not enough to modify only the periphery to utilize an ELSD for miniaturized applications; the components from nebulization to the optical detector must also be optimized. For the ELSD, an *S/N* of 169 was achieved.

For the different ESI–MS emitter tip capillaries, an *S/N* of $2.7 * 10^3$, $2.5 * 10^3$, and $3.0 * 10^3$ was determined with decreasing ID. Normally, at a constant injection volume and constant concentration of the analyte, the *S/N* should decrease with increasing emitter ID due to a higher extra-post-column volume and the resulting additional band broadening. This is not the case here and can be explained by the different surface roughness of the emitters. The ESI–MS emitter with an ID of 65 μm is completely made of stainless steel while the other two emitters are made of PEEKsil™, and only the tip of these emitters is made of stainless steel. This in turn can lead to flow turbulences which influence the laminar flow at the wall region and have a negative effect on dispersion [16, 23]. In direct comparison of the ESI–MS emitter configurations, no influence on the peak symmetry could be observed.

As expected, the mass flow–dependent detectors are superior in direct *S/N* comparison to the concentration-dependent detector. It should also be noted that by simple modifications such as changing the nebulizer chamber of the ELSD or the simple change of the emitter tip ID of the ESI source, a successful coupling of conventional scale detector systems with MicroLC was achieved. This can contribute to the accelerating of the spread of miniaturized systems.

Conclusion

The assumption that only the cell volume of concentration-dependent detectors needs to be considered when determining the efficiency is a misconception. Due to the variety of detector designs, cell geometries, and the associated changes in the inner diameters and turns of the flow path, it can be concluded that there is no linear relationship between band broadening and extra-post-column volume. The comparison of the two UV detectors used in this study demonstrates that even if the modular design is retained, a reduction of the extra-post-column volume is possible using optical waveguides. If the volume is set in relation to the signal-to-noise ratio, it becomes clear that the efficiency gain outweighs the lower volume. In addition, it could be shown that a change to a larger capillary ID after the transfer capillary behind the column has a negative effect on the efficiency. This effect occurred especially at high flow rates as shown for the FLD and the ESI–MS emitter tip with an ID of 65 μm. In addition, the usable flow rate range can be shifted to lower flow rates by reducing the emitter tip ID. No negative influence was observed with a reduction of the diameter after the post-column transfer capillary ID. As assumed, the comparison of the MS setups clearly shows that by simply changing the ESI–MS emitter capillary, a conventional ion source can be used for miniaturized LC. This does not apply to the ELSD where, despite the use of a micro nebulizer, the evaporation area should also be optimized for the benefit of higher chromatographic efficiency. The investigated detector concepts also underline that the classical approach of "HiFi Tower" HPLC systems is no longer appropriate to fully utilize the intrinsic efficiency of sub-2-μm particle packed columns. Especially in the field of miniaturized HPLC, where the reduction of the extra-column volumes is of particular importance, systems should be used in which the individual components, e.g., pumps, valves, connecting tubing, and transfer capillaries, are fine-tuned to each other.

CRediT authorship contribution statement Tobias Werres: conceptualization, investigation, visualization, project administration, writing—original draft; Thorsten Teutenberg: funding acquisition, supervision, writing—review & editing; Torsten C. Schmidt: supervision, writing—review and editing.

Declarations

Conflict of interest The authors declare no competing interests.

References

1. Vargas Medina DA, Maciel EVS, de Toffoli AL, Lanças FM. Miniaturization of liquid chromatography coupled to mass spectrometry.: 2. Achievements on modern instrumentation for miniaturized liquid chromatography coupled to mass spectrometry. TrAC - Trends Anal Chem. 2020;128:115910. https://doi.org/10.1016/j.trac.2020.115910.

2. Mejía-Carmona K, da Silva Soares, Burato J, Borsatto JVB, de Toffoli AL, Lanças FM. Miniaturization of liquid chromatography coupled to mass spectrometry: 1. Current trends on miniaturized LC columns. TrAC - Trends Anal Chem. 2020;122:115735. https://doi.org/10.1016/j.trac.2019.115735.

3. Agrawal A, Keçili R, Ghorbani-Bidkorbeh F, Hussain CM. Green miniaturized technologies in analytical and bioanalytical chemistry. TrAC Trends Anal Chem. 2021;143: 116383. https://doi.org/10.1016/j.trac.2021.116383.

4. Napolitano-Tabares PI, Negrín-Santamaría I, Gutiérrez-Serpa A, Pino V. Recent efforts to increase greenness in chromatography. Curr Opin Green Sustain Chem. 2021;32: 100536. https://doi.org/10.1016/j.cogsc.2021.100536.

5. Bian Y, Zheng R, Bayer FP, Wong C, Chang YC, Meng C, Zolg DP, Reinecke M, Zecha J, Wiechmann S, Heinzlmeir S, Scherr J, Hemmer B, Baynham M, Gingras AC, Boychenko O, Kuster B. Robust, reproducible and quantitative analysis of thousands of proteomes by micro-flow LC–MS/MS. Nat Commun. 2020;11:1–12. https://doi.org/10.1038/s41467-019-13973-x.

6. Vehus T, Roberg-Larsen H, Waaler J, Aslaksen S, Krauss S, Wilson SR, Lundanes E. Versatile, sensitive liquid chromatography mass spectrometry-Implementation of 10 μm OT columns suitable for small molecules, peptides and proteins. Sci Rep. 2016;6:1–10. https://doi.org/10.1038/srep37507.

7. Hetzel T, vom Eyser C, Tuerk J, Teutenberg T, Schmidt TC. Micro-liquid chromatography mass spectrometry for the analysis of antineoplastic drugs from wipe samples. Anal Bioanal Chem. 2016;408:8221–9. https://doi.org/10.1007/s00216-016-9932-y.

8. Vanderlinden K, Broeckhoven K, Vanderheyden Y, Desmet G. Effect of pre- and post-column band broadening on the performance of high-speed chromatography columns under isocratic and gradient conditions. J Chromatogr A. 2016;1442:73–82. https://doi.org/10.1016/j.chroma.2016.03.016.

9. Broeckhoven K, Desmet G. The future of UHPLC: towards higher pressure and/or smaller particles? TrAC Trends Anal Chem. 2014;63:65–75. https://doi.org/10.1016/j.trac.2014.06.022.

10. Rahimi F, Chatzimichail S, Saifuddin A, Surman AJ, Taylor-Robinson SD, Salehi-Reyhani A. A review of portable high-performance liquid chromatography: the future of the field? Berlin Heidelberg: Springer; 2020.

11. Lam SC, Coates LJ, Hemida M, Gupta V, Haddad PR, Macka M, Paull B. Miniature and fully portable gradient capillary liquid chromatograph. Anal Chim Acta. 2020;1101:199–210. https://doi.org/10.1016/j.aca.2019.12.014.

12. Sharma S, Plistil A, Barnett HE, Tolley HD, Farnsworth PB, Stearns SD, Lee ML. Hand-portable gradient capillary liquid chromatography pumping system. Anal Chem. 2015;87:10457–61. https://doi.org/10.1021/acs.analchem.5b02583.

13. Lankelma J, van Iperen DJ, van der Sluis PJ. Towards using high-performance liquid chromatography at home. J Chromatogr A. 2021;1639: 461925. https://doi.org/10.1016/j.chroma.2021.461925.

14. Su C-K. Review of 3D-Printed functionalized devices for chemical and biochemical analysis. Anal Chim Acta. 2021;1158: 338348. https://doi.org/10.1016/j.aca.2021.338348.

15. Balakrishnan HK, Doeven EH, Merenda A, Dumée LF, Guijt RM. 3D printing for the integration of porous materials into miniaturised fluidic devices: a review. Anal Chim Acta. 2021;338796. https://doi.org/10.1016/j.aca.2021.338796.

16. Desmet G, Broeckhoven K. Extra-column band broadening effects in contemporary liquid chromatography: causes and solutions. TrAC - Trends Anal Chem. 2019;119: 115619. https://doi.org/10.1016/j.trac.2019.115619.

17. Hetzel T, Loeker D, Teutenberg T, Schmidt TC. Characterization of the efficiency of microbore liquid chromatography columns by van Deemter and kinetic plot analysis. J Sep Sci. 2016;39:3889–97. https://doi.org/10.1002/jssc.201600775.

18. Chester TL. Recent developments in high-performance liquid chromatography stationary phases. Anal Chem. 2013;85:579–89. https://doi.org/10.1021/ac303180y.

19. Werres T, Schmidt TC, Teutenberg T. The influence of injection volume on efficiency of microbore liquid chromatography columns for gradient and isocratic elution. J Chromatogr A. 2021;1641. https://doi.org/10.1016/j.chroma.2021.461965.

20. Taylor G. Dispersion of soluble matter in solvent flowing slowly through a tube. Proc R Soc London Ser A Math Phys Sci. 1953;219:186–203. https://doi.org/10.1098/rspa.1953.0139.

21. Aris R. On the dispersion of a solute in a fluid flowing through a tube. Proc R Soc London Ser A Math Phys Sci. 1956;235:67–77. https://doi.org/10.1098/rspa.1956.0065.

22. He B, Tait N, Regnier F. Fabrication of nanocolumns for liquid chromatography. Anal Chem. 1998;70:3790–7. https://doi.org/10.1021/ac980028h.

23. Filip B, Bochenek R, Baran K, Strzałka D, Antos D. Influence of the geometry of extra column volumes on band broadening in a chromatographic system. Predictions by computational fluid dynamics. J Chromatogr A. 2021;1653:462410. https://doi.org/10.1016/j.chroma.2021.462410.

24. Gunnarson C, Lauer T, Willenbring H, Larson E, Dittmann M, Broeckhoven K, Stoll DR. Implications of dispersion in connecting capillaries for separation systems involving post-column flow splitting. J Chromatogr A. 2021;1639: 461893. https://doi.org/10.1016/j.chroma.2021.461893.

25. Desmet G, Cabooter D, Broeckhoven K. Graphical data representation methods to assess the quality of LC columns. Anal Chem. 2015;87:8593–602. https://doi.org/10.1021/ac504473p.

26. Spaggiari D, Fekete S, Eugster PJ, Veuthey JL, Geiser L, Rudaz S, Guillarme D. Contribution of various types of liquid chromatography-mass spectrometry instruments to band broadening in fast analysis. J Chromatogr A. 2013;1310:45–55. https://doi.org/10.1016/j.chroma.2013.08.001.